Observations of Anomalous Cosmic Rays at 1 AU

R. A. Leske[1], R. A. Mewaldt[1], E. R. Christian[2], C. M. S. Cohen[1], A. C. Cummings[1], P. L. Slocum[3], E. C. Stone[1], T. T. von Rosenvinge[2], and M. E. Wiedenbeck[3]

[1]*California Institute of Technology, Pasadena, CA 91125 USA*
[2]*NASA/Goddard Space Flight Center, Greenbelt, MD 20771 USA*
[3]*Jet Propulsion Laboratory, Pasadena, CA 91109 USA*

Abstract. Anomalous cosmic rays (ACRs) provide a sensitive probe of the access of energetic particles to the inner heliosphere, varying in intensity by more than two orders of magnitude during the course of the solar cycle. New data which are becoming available from the Advanced Composition Explorer (ACE) can provide a detailed record of ACR intensity and spectral changes on short ($\sim$ 1 day) time scales during the approach to solar maximum, which will help address issues of ACR modulation and transport. The elemental and isotopic composition of ACRs provides important information on the source or sources of these particles, while their ionic charge state composition and its energy dependence serves as a diagnostic of their acceleration time scale. We review measurements of the ACR elemental, isotopic, and charge state composition and spectra as determined at 1 AU by SAMPEX, ACE, Wind, and other spacecraft. These results are important input to models of the acceleration, modulation, and transport of ACRs.

INTRODUCTION

Anomalous cosmic rays (ACRs) were discovered some 25 years ago as unexpected intensity enhancements in low energy quiet time He, N, and O spectra (1, 2, 3), with a composition quite unlike that previously seen in other samples of energetic particles. Although the correct interpretation of these particles was suggested very soon after their discovery, verification of the model has taken much longer. In the standard scenario (4, 5), most ACRs begin in the interstellar medium (ISM) as neutral atoms that flow relatively unimpeded into the heliosphere, where they become ionized by solar UV or by charge exchange with the solar wind as they approach the Sun. Once singly ionized, they are convected into the outer heliosphere by the solar wind as "pickup" ions and carried to the solar wind termination shock, where they are accelerated to energies of several to tens of MeV/nucleon and become the ACRs observed throughout the heliosphere.

Many predictions of this model have now been confirmed experimentally. Other elements likely to be primarily neutral in the ISM due to their high first ionization potential (FIP), such as H (6), Ne (7), and Ar (8), are now known to have an ACR component; neutral interstellar He has been found flowing into the heliosphere (9); pickup ions have been detected (10) with a composition consistent with an origin as interstellar neutrals (11); and low energy ACRs have been shown to be predominantly singly ionized (12, 13). The distribution of ACRs within the heliosphere, both radially and latitudinally (e.g., (14, 15)), the reversal of the latitudinal gradients when the solar magnetic field changes polarity (16), and the continually unfolding spectra seen by Voyager 1 as it approaches the termination shock (17) also agree with the general expectations of the standard model.

Recently, some low-FIP elements not expected to be neutral in the ISM have been found to exhibit ACR-like enhancements (18, 19, 20). Also, above $\sim$ 20 MeV/nucleon, ACRs have been shown to be mainly multiply ionized instead of singly charged (21, 22). Such findings may lead to some extensions to the standard scenario and have prompted revisions in models of the acceleration and transport of ACRs in the heliosphere (23, 24, 25).

In this article, we review measurements of ACRs made during the past solar minimum with new spacecraft at 1 AU, in particular the Solar, Anomalous, and Magnetospheric Particle Explorer (SAMPEX) in a polar orbit about the Earth, Wind in the nearby interplanetary medium, and the Advanced Composition Explorer (ACE) in orbit about the upstream Sun-Earth Lagrange point L_1. We discuss ACR temporal variations and their elemental, isotopic, and especially charge state spectra.

TIME VARIABILITY

Studies of ACRs at 1 AU are essentially limited to solar minimum periods. As shown in Figure 1, the intensity

CP528, *Acceleration and Transport of Energetic Particles Observed in the Heliosphere: ACE 2000 Symposium,*
edited by Richard A. Mewaldt, et al.

of ACRs varies by a factor of ~ 100 over the course of the solar cycle, with ACRs becoming undetectable above the galactic cosmic ray (GCR) or solar particle backgrounds at 1 AU during solar maximum. These intensity variations tend to track those seen in the modulation of GCRs, as reflected in the variations in the neutron monitor count rate, although the ACR intensity recovered more quickly than the GCRs at the onset of the last solar minimum (26).

The data in Figure 1 are averaged over periods of a solar rotation or longer. Using the Solar Isotope Spectrometer (SIS) on ACE, with its large (~ 40 cm^{2}sr) collecting power (27), it is possible to obtain more detailed records of ACR time variability and even track day-to-day variations in ACR intensity, as illustrated in Figure 2. These data were selected for solar quiet days (when the 3.4–7.3 MeV/nucleon He intensity was $< 10^{-4}$ (cm^2·sr·s·MeV/nuc)$^{-1}$) and have had the GCR background subtracted. This background correction was $\lesssim 5\%$ early in the period, and grew to $\sim 30\%$ by the end of the period. The ACR variability is considerable, with factors of ~ 5 intensity fluctuations sometimes observed during half a solar rotation (e.g., near day 200 of 1999), possibly due to modulation by solar wind structures (28). Even on these short time scales, the correlation between the ACR intensity and the Climax neutron monitor count rate is evident. These new ACE data, publicly available from the ACE Science Center (*http://www.srl.caltech.edu/ACE/ASC*), will provide new challenges and tests for modulation models.

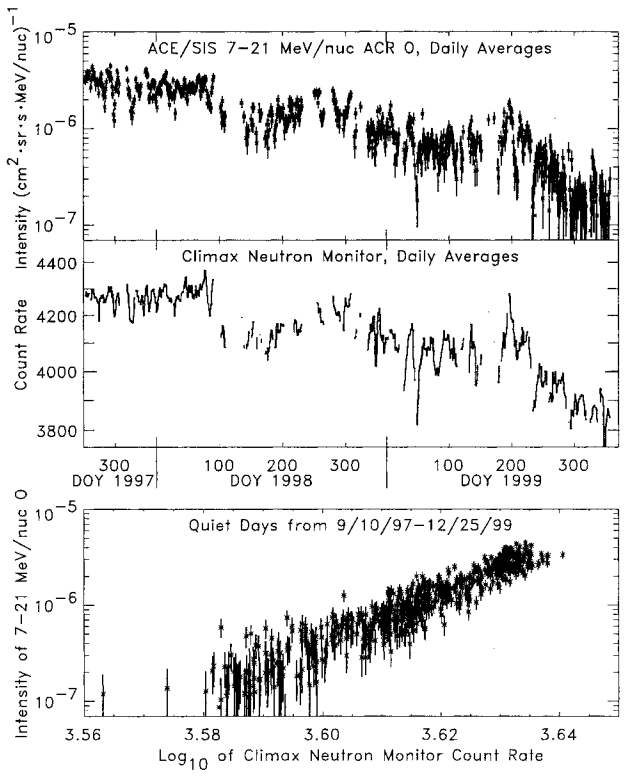

FIGURE 2. Time dependence of the daily average quiet time fluxes of 7–21 MeV/nucleon O from SIS (*top*) and the count rate of the Climax neutron monitor (*middle*). The two quantities are strongly correlated, as indicated in the cross plot (*bottom*).

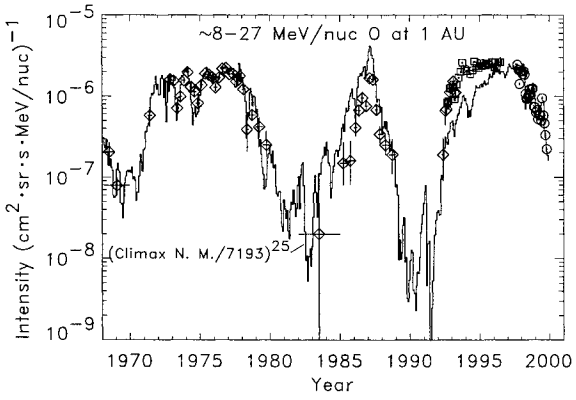

FIGURE 1. Quiet time intensities of $\sim$ 8–27 MeV/nucleon ACR O at 1 AU over the past 3 solar cycles (*data points*), compared with the Bartels rotation averaged count rate of the Climax neutron monitor scaled as indicated (*histogram*). Recent ACR data are from SAMPEX (*squares*) and from SIS on ACE (*circles*); earlier data (*diamonds*) are from OGO-5 (29, 30) and IMP 6 (7) for 1968-1971, and IMP 7 and 8 (26) for 1972-1992.

The ACR intensity is falling dramatically as the maximum of solar cycle 23 approaches, and the amount of modulation is energy dependent, as shown in Figure 3. Since the launch of ACE, the intensity of ACR O at 1 AU at an energy of 10 MeV/nucleon has fallen by a factor of ~ 20. ACR O is still present, however, as indicated by the low energy turn up (although the very lowest energy point may have some residual contamination from solar particles during the latest period). GCR O, on the other hand, has so far decreased by only a factor of ~ 2 at 100 MeV/nucleon. This is due largely to the fact that 100 MeV/nucleon is below the peak of the GCR intensity, and adiabatically cooled particles from higher energies fill in for the particles lost from lower energies. The ACRs at ~ 10 MeV/nucleon, on the other hand, are well above the peak of the steeply falling ACR spectrum, and fewer higher energy particles are available to compensate for the low energies losses (28). Also, the velocity of 100 MeV/nucleon GCRs is more than 3 times that of 8 MeV/nucleon ACRs, even though the rigidity of these fully ionized nuclei is less than half that of the singly ionized ACRs. If the diffusion coefficient scales as the product of velocity and a weak function of rigidity (see, e.g., (31)), the GCRs have a larger diffusion coefficent which also results in less solar modulation than for ACRs.

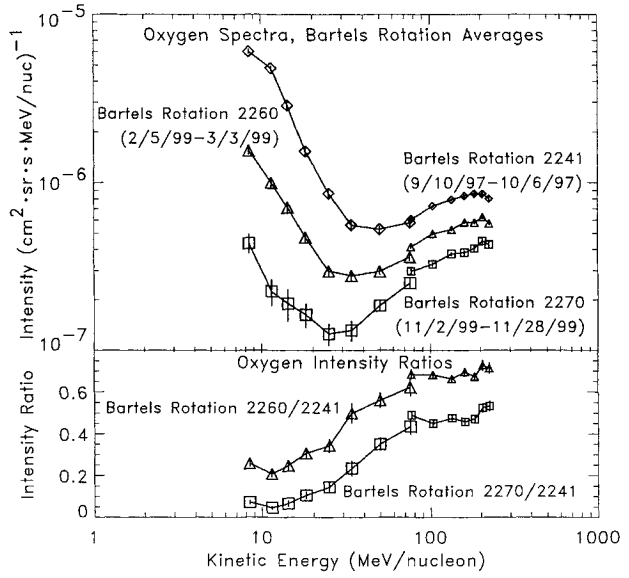

FIGURE 3. Temporal evolution of O spectra during the approach to solar maximum is illustrated for 3 selected Bartels rotations (*top*), using data from SIS (*larger symbols*) and CRIS (*smaller symbols* above ~ 80 MeV/nucleon) on ACE. Modulation differences with energy are more clearly illustrated by the intensity ratios (*bottom*).

ELEMENTAL AND ISOTOPIC SPECTRA

Elemental spectra of ACRs during solar minimum are illustrated in Figure 4, combining data from SIS, higher energy data from the Cosmic Ray Isotope Spectrometer (CRIS) on ACE (32) and lower energy data from the Low-Energy Matrix Telescope (LEMT) on Wind (19). The ACE data were accumulated during quiet days from 8/27/97 through 3/23/98, when ACR fluxes were high and relatively constant (see Figure 2). The Wind data set used here runs from November 1994 to April 1998, with most of the quiet time periods occurring in 1996 and early 1997 when the ACR fluxes were similar to those during the ACE analysis period (19). The agreement between measurements from all three instruments represented in Figure 4 is remarkably good in general. These combined spectra represent the best ACR spectra at 1 AU obtained to date (compared, e.g., with (33)).

The ACR low energy intensity enhancements are clearly exhibited for N, O, Ne, and Ar in Figure 4, but for other elements the turn-up, if present, is much smaller and starts at lower energies. In particular, the ACR C abundance is somewhat controversial. Other observations at 1 AU from SAMPEX (26) and Geotail (34) have found a rather large amount of ACR-like C present, with C/O ~ 0.1, but further observations from SAMPEX (35, 36) indicate that most of this C is not singly ionized. The Wind results (19) suggest that the C turn-up is greatly reduced when tighter quiet time cuts are imposed, but large instrumental background corrections were necessary for C, and the resulting spectrum is inconsistent at higher energies by a factor of 2 with results from SIS (which may also have some background at the lowest energies). The question of just how much ACR C is present at 1 AU under strict quiet time conditions appears to be unresolved.

Turn-ups at energies < 5 MeV/nucleon in the spectra of the low-FIP elements Mg, Si, and S from Wind (19) seem to be larger relative to ACR O, Ne, or Ar than those found in the outer heliosphere by Voyager, suggesting that other sources besides interstellar neutrals may contribute to these species at 1 AU (20). Other than the possibility of contamination from particles accelerated at corotating interaction regions, potential contributors to this population of low-FIP elements include an "inner source" from adsorbed, neutralized, and desorbed solar wind on interplanetary dust grains (37) or grain destruction products (38), or solar wind reaccelerated at the termination shock (39).

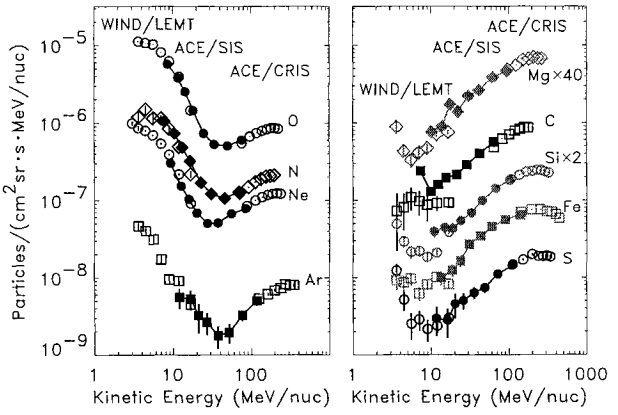

FIGURE 4. Elemental spectra taken from (40), using data from the SIS (*filled symbols*) and CRIS (*high energy open symbols*) instruments on ACE (41) and from the LEMT instrument (*low energy open symbols*) on Wind (19). The statistical uncertainties shown are often much smaller than the plotted symbols.

Besides elemental spectra, recent ACR results from ACE include isotopic spectra of ACR N, O, and Ne, as shown in Figure 5 (40). The isotopic abundances are quite different for ACRs and GCRs. In GCRs, relatively large quantities of ^{15}N, ^{18}O, and ^{21}Ne are produced by cosmic ray spallation during transport through the Galaxy, so the observed abundances are not directly representative of the GCR source. Unlike GCRs, the ACRs have passed through a negligible amount of material, and no secondary spallation products should be present.

In addition to large ACR turn-ups of the dominant isotopes ^{14}N, ^{16}O, and ^{20}Ne, the rarer species ^{18}O and ^{22}Ne also show clear low-energy ACR enhancements (40). The

ACR $^{18}O/^{16}O$ and $^{22}Ne/^{20}Ne$ ratios are consistent with those found in solar system material (42), with the Ne isotopic composition more closely resembling that found in the solar wind (43) than that present in other meteoritic components (see, e.g., (44)). The ACR $^{22}Ne/^{20}Ne$ ratio, which should represent the ratio in the local ISM, is a factor of ~ 5 below that deduced for the GCR source (see, e.g., (45, 46)), indicating that GCRs cannot be only an accelerated sample of the local ISM (40, 47). The lack of low energy enhancements in the spectra of ^{15}N and ^{21}Ne suggest that the ACR $^{15}N/^{14}N$ and $^{21}Ne/^{20}Ne$ ratios are no more than 5 and ~ 10 times, respectively, those found in standard solar system abundances (42).

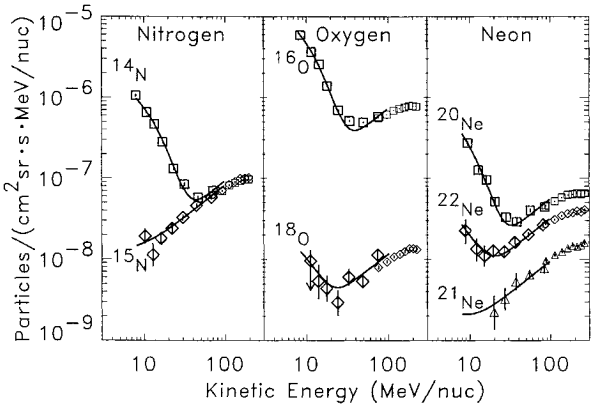

FIGURE 5. SIS quiet time isotopic energy spectra from 8/97-3/98 for N (*left*), O (*center*), and Ne (*right*); smaller symbols above ~ 80 MeV/nucleon are from CRIS (N. E. Yanasak, private communication). Curves show the sum of power law spectra ($\propto (E/M)^{0.8}$) fit to the SIS GCR data and exponential spectra drawn through the ACR isotopes, with the ACR relative abundances of the rarer heavy isotopes for each element assumed to be the same as those found in solar system material (42).

CHARGE STATE COMPOSITION

Although of great interest for determining the isotopic composition of the neutral component of the ISM and possibly for helping to constrain the estimation of mass-dependent acceleration efficiencies, the presence of heavier isotopes of ACR O and Ne has little effect on the overall shape of the elemental spectra, as their abundances are low and their rigidities differ by only 10% from those of the dominant isotopes. A recent finding which has a much more critical impact on understanding ACR acceleration and transport has been the determination of their charge state composition as a function of energy (12, 13, 21). ACE and Wind cannot make such measurements, as the only method available at present to directly determine charge states at ACR energies requires the use of the Earth's magnetic field as a particle rigidity filter. This in turn requires a spacecraft in a high inclination or polar Earth orbit, such as SAMPEX.

The geomagnetic filter effect is illustrated in Figure 6, which shows the kinetic energy vs. invariant latitude for O particles detected by the Mass Spectrometer Telescope (MAST) on SAMPEX. (The invariant latitude, Λ, is the magnetic latitude at which a given field line intersects the Earth's surface and is related to the magnetic L shell by $\cos^2\Lambda = 1/L$; see, e.g., (48)). The abrupt drop in density at high energies below $\sim 60°$ is due to the fact that fully stripped particles at these energies have a rigidity too low to penetrate the geomagnetic field to lower latitudes. Singly charged particles have a higher rigidity than fully stripped particles at the same kinetic energy and exhibit a similar "cutoff" at lower latitudes. (Geographic longitudes at which trapped O is found (49) have not been included in this figure). Although GCR O nuclei are abundant at high latitudes throughout the entire energy interval sampled by MAST, they are quite effectively excluded at latitudes below the geomagnetic cutoff for fully stripped ($Q = 8$) oxygen, leaving only the ACRs extending to these lower latitudes.

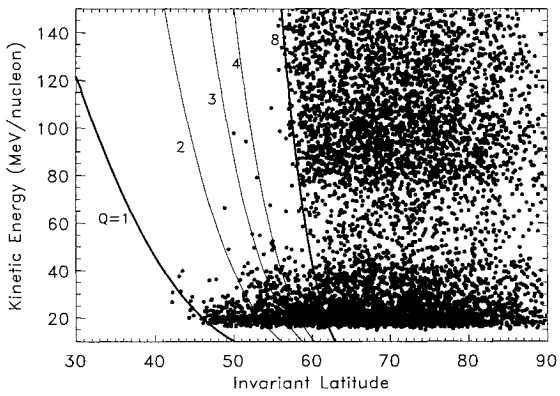

FIGURE 6. Kinetic energy vs. invariant latitude for quiet time O particles measured by MAST/SAMPEX, as in (21). The low density region from $\sim$ 45–75 MeV/nucleon is due to a detector failure part way through the mission, while the decreasing density towards higher latitudes ($\gtrsim 80°$) reflects the lesser amount of time spent at such latitudes in SAMPEX's 82° inclination orbit. Curves show the calculated approximate locations of the geomagnetic cutoffs for O with the charge states (Q) indicated, based on an empirically derived cutoff-rigidity relation (50).

Energy spectra obtained using only those particles which penetrate more than several degrees below the cutoff for fully stripped nuclei are shown in Figure 7. The geomagnetic filter approach allows the pure ACR component to be revealed even in the presence of an interplanetary background of GCRs with intensity $\gtrsim 100$ times greater. Combined with MAST's ability to resolve isotopes, this powerful background suppression has also been used to study the isotopic composition of pure ACRs

(47), complementing the results from ACE (Figure 5) which have better statistical accuracy but require GCR background corrections.

Separated from the GCR background in Figure 7, ACRs are seen to extend to energies of at least $\sim$ 100 MeV/nucleon with smoothly falling spectra. The diffusive shock-drift ACR acceleration model (31) predicts that the "maximum" energy gain ΔE (beyond which the spectrum is expected to fall off rapidly) for a particle of charge Qe at a quasi-perpendicular shock is $\Delta E \simeq Qe\Delta\phi$, where $\Delta\phi$ is the change in potential in drifting along the shock. Jokipii (31) calculates that $\Delta\phi \simeq 240$ MV between the heliospheric equator and pole for the termination shock, which implies that the spectrum of singly charged ^{16}O should steepen significantly beyond $\sim$ 15 MeV/nucleon. Conversely, as pointed out by Mewaldt et al. (35), ^{16}O with a higher charge state would be more easily accelerated to the observed $\sim$ 100 MeV/nucleon.

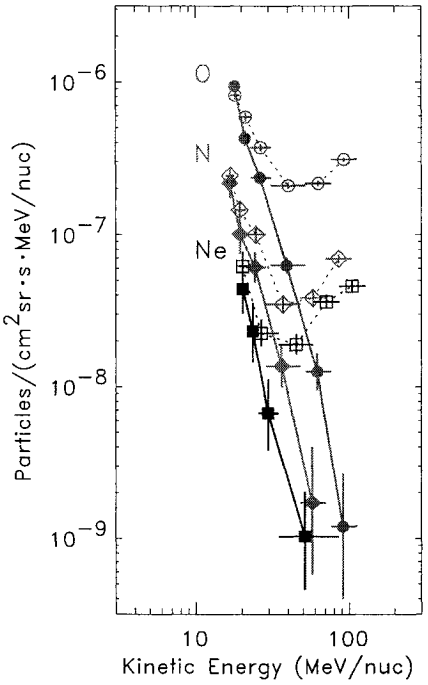

FIGURE 7. MAST/SAMPEX energy spectra of pure ACR N, O, and Ne (*filled symbols; solid lines*) obtained using the geomagnetic filter approach, compared with interplanetary spectra at $\Lambda > 65°$ (*open symbols; dotted lines*) measured by MAST during the same time period (7/6/92-1/7/95), as in (35).

Only an upper limit on the charge state of any individual particle can be determined using the geomagnetic filter technique, not the actual charge state itself. However, the distribution in latitude of a collection of particles does reveal the charge state composition of the sample. For example, none of the events in Figure 6 around 30–40 MeV/nucleon between the $Q = 2$ and $Q = 3$ cutoffs could have $Q > 2$, or else they could not be found at such low latitudes, but any particular event might have either $Q = 1$ or $Q = 2$. However, the significant drop in density below the $Q = 2$ cutoff shows that most of these events must in fact be doubly ionized, and the relative densities on either side of the $Q = 2$ cutoff indicate the relative proportions of singly and doubly ionized particles at this energy.

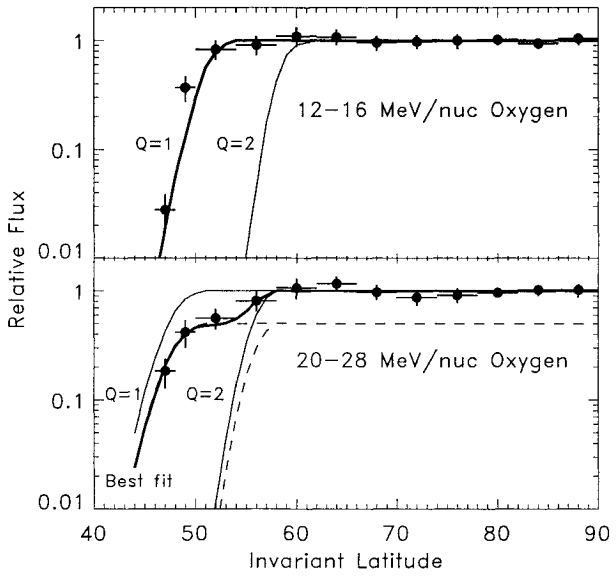

FIGURE 8. Relative flux profiles (normalized to 1 at high latitudes) as a function of invariant latitude for O at 12–16 MeV/nucleon (*top*) and 20–28 MeV/nucleon (*bottom*) from HILT/SAMPEX (13, 22), using quiet time periods between October 1992 and January 1995. Curves show the calculated profiles for particles with $Q = 1$ and $Q = 2$, and the weighted sum of these profiles (equal to the sum of the dashed curves) which best fits the high energy data.

The process of obtaining charge state distributions using the geomagnetic filter is illustrated more quantitatively in Figure 8, which shows how the O flux varies with latitude at two different energies measured by the Heavy Ion Large Telescope (HILT) on SAMPEX (13, 22). Although variations in geomagnetic activity or the arrival directions of the particles may produce some blurring of the cutoff locations, the expected difference in cutoff latitude for O with $Q = 1$ and $Q = 2$ (Figures 6 and 8) is so large that these effects are relatively unimportant. (Such effects have a greater impact when using this same technique to study solar energetic particle charge states as in (51), where the charge states are much higher and the cutoffs for different Q more closely spaced.) Below 16 MeV/nucleon, the flux profile with respect to latitude agrees with that expected for $Q = 1$ particles (13). However, at the higher energies, there is a pronounced dip in the profile at low latitudes starting near the expected position of the $Q = 2$ cutoff. The data are well fit by the

sum of two step profiles of roughly equal height, one extending to the $Q = 1$ cutoff, the other only to the $Q = 2$ cutoff latitude, indicating a mixture of equal amounts of both charge states at these energies.

Similar analyses of MAST data (21, 52) yield the O charge state spectra shown in Figure 9. Singly charged O is seen to have a very steep spectrum, possibly with a break at $\sim$ 20–30 MeV/nucleon, and only the higher charge states are accelerated to higher energies, in general agreement with the diffusive shock-drift acceleration model (53). The abundances of higher charged ACRs appear to be consistent with those expected to be produced by electron stripping during acceleration, if the timescale for acceleration to 10 MeV/nucleon is $\sim$ 1 year (21).

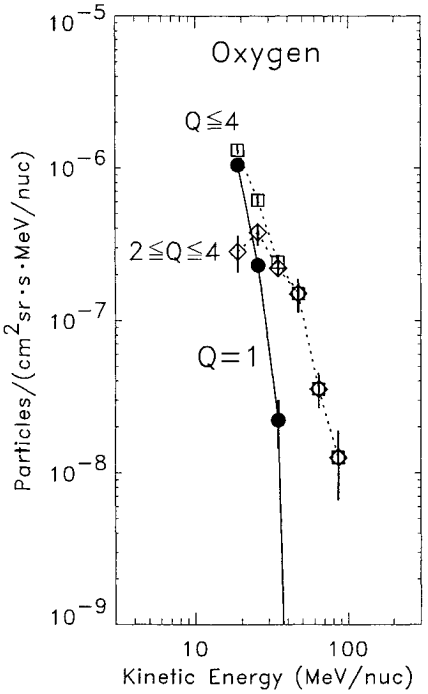

FIGURE 9. Energy spectra of ACR O^+ (*filled circles*) compared with the spectra of $O^{+2}+O^{+3}+O^{+4}$ (*open diamonds*) and their sum, $O^{+}+O^{+2}+O^{+3}+O^{+4}$ (*open squares*), from (52). Differences in the $Q \leq 4$ spectrum shown here and the filtered O spectrum in Figure 7 arise from the assumption made in the earlier work (35) that ACRs are singly ionized at all energies, which would significantly increase the size of the latitude interval over which they could be detected (Figure 6) and hence the effective collection time.

Carrying out the same analysis for N and Ne in addition to O (22, 52), it is found that in each case the fraction of ACRs that is singly ionized decreases rapidly with increasing energy. The energy dependence of the singly ionized fraction seems better organized by total energy as in Figure 10 than by energy per nucleon (33). Above energies of $25.5 \pm 2.5, 22 \pm 2$, and 17.5 ± 2.0 MeV/nucleon for N, O, and Ne, respectively, more than half the ACRs are *not* singly ionized and multiply charged ACRs dominate (33). This corresponds to a common total energy of $\sim$ 350 MeV for all three species, which again supports the diffusive shock-drift acceleration picture (23). Attempts to model and understand this transition to higher charge states in more detail are ongoing (23, 24).

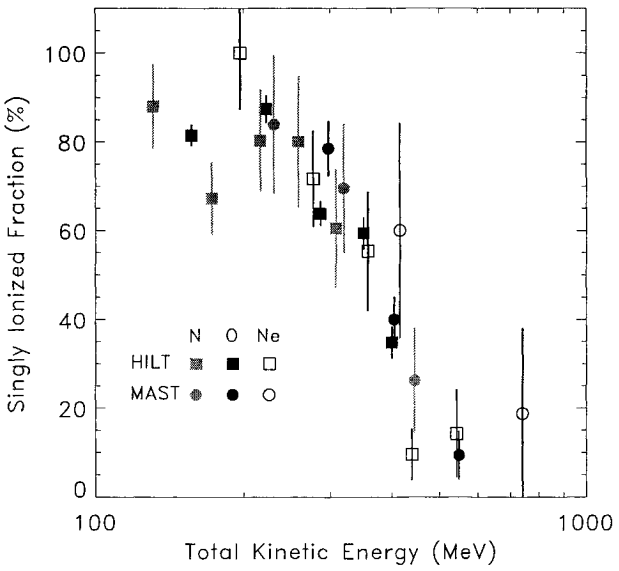

FIGURE 10. Singly ionized fraction of ACR N (*filled gray symbols*), O (*filled black symbols*), and Ne (*open symbols*) as a function of total energy, combining data from HILT (*squares*; (22)) and MAST (*circles*; (52)) on SAMPEX. Adapted from (33).

GEOMAGNETICALLY TRAPPED ACRS

One population of ACR particles unique to 1 AU (or, more specifically, low Earth orbit) is found in the Earth's radiation belts (49, 54, 55). Singly charged ACRs can penetrate to lower latitudes in the magnetosphere than fully stripped nuclei and may lose some or all of their electrons if they pass through the thin upper reaches of the atmosphere. Particles with the correct combination of energy and pitch angle relative to the magnetic field entering at latitudes near the $Q = 1$ cutoff will be stably trapped in the geomagnetic field after this abrupt change in their rigidity (56) and form a radiation belt around $L = 2$ (which would appear near $\Lambda = 45°$ straddling the $Q = 1$ cutoff line in Figure 6).

The trapped ACRs are potentially attractive for ACR studies because they are concentrated in the radiation belt to intensities $\sim$ 100 times greater than normally found in interplanetary space at 1 AU (57). Like the geomagnetically filtered ACRs described above, this is a pure sample of ACRs, free of GCR or solar particle backgrounds. Their elemental abundances are depleted in C, N, and per-

haps Ne relative to O (57). This may be due to differences between the elements in their electron stripping cross sections or the fact that ions with more electrons to lose can undergo a greater change in rigidity during stripping and should be more likely to be trapped (57). Their composition is also influenced by the fact that only the singly-ionized fraction should be able to penetrate to $L = 2$ and become trapped. Indeed, the trapped ACR energy spectra are observed to be very similar to those of the singly-ionized components and are much softer than those of the overall filtered ACRs (57). Their isotopic composition is similar to that found in interplanetary ACRs but with higher statistical accuracy (47). Finally, the trapped ACR intensity seems to track the variations seen in interplanetary ACRs (54, 57), even reflecting the recent decreases shown in Figure 2 as solar maximum approaches (58). It will be interesting to see if ACRs are still detectable in this distilled sample long after they have faded beneath the GCR background in interplanetary space.

SUMMARY

The presently declining ACR fluxes at 1 AU mark the close of a solar cycle minimum during which tremendous progress has been made in both measuring and understanding these particles. The elemental spectra have been determined more precisely than ever before and have revealed new species with ACR-like enhancements, possibly with different origins and histories than the "classic" ACRs. Measurements of their isotopic composition are beginning to be made, which may provide insight into the nucleosynthetic history of the ISM. The GCR background has been stripped away to uncover previously unsuspected ACRs out to energies as high as 100 MeV/nucleon, indicating that the termination shock is capable of accelerating particles to a total energy as great as 1.6 GeV. Clues as to how such high energies are achieved were provided by the revelation that high energy ACRs are multiply charged, which can also help to constrain the acceleration time scale, while low energy ACRs have been confirmed to be singly ionized as predicted.

Measurements utilizing the large collecting power of instruments on Wind and ACE, or taking advantage of the geomagnetic filter or the concentrated collection of trapped ACRs with SAMPEX, may allow ACR intensities to be tracked longer into solar maximum than in previous cycles, furthering studies of ACR modulation under extreme conditions. While theorists incorporate the recent results into their latest models to improve our understanding of ACRs, we eagerly anticipate the return of these particles to 1 AU around 2003 and the discoveries yet to come during the next solar minimum.

ACKNOWLEDGMENTS

This research was supported by NASA at the California Institute of Technology (under grant NAG5-6912), the Jet Propulsion Laboratory, and the Goddard Space Flight Center. We thank R. S. Selesnick, N. E. Yanasak, and B. Klecker for providing data used in some of the figures. Climax neutron monitor data were obtained from the web, courtesy of the University of Chicago, National Science Foundation grant ATM-9613963.

REFERENCES

1. Garcia-Munoz, M., Mason, G. M., and Simpson, J. A., *Astrophys. J. Letters* **182**, L81-L84 (1973).
2. Hovestadt, D., Vollmer, O., Gloeckler, G., and Fan, C. Y., *Phys. Rev. Lett.* **31**, L650-L653 (1973).
3. McDonald, F. B., Teegarden, B. J., Trainor, J. H., and Webber, W. R., *Astrophys. J. Letters* **187**, L105-L108 (1974).
4. Fisk, L. A., Kozlovsky, B., and Ramaty, R., *Astrophys. J. Letters* **190**, L35-L37 (1974).
5. Pesses, M. E., Jokipii, J. R., and Eichler, D., *Astrophys. J. Letters* **246**, L85-L88 (1981).
6. Christian, E. R., Cummings, A. C., and Stone, E. C., *Astrophys. J. Letters* **334**, L77-L80 (1988).
7. von Rosenvinge, T. T. and McDonald, F. B., *Proc. 14th Internat. Cosmic Ray Conf. (Munich)* **2**, 792-797 (1975).
8. Cummings, A. C. and Stone, E. C., *Proc. 20th Internat. Cosmic Ray Conf. (Moscow)* **3**, 413-416 (1987).
9. Witte, M., Rosenbauer, H., Banaszkiewicz, M., and Fahr, H., *Adv. Space Res.* **13**, 121-130 (1993).
10. Möbius, E., Hovestadt, D., Klecker, B., Scholer, M., Gloeckler, G., and Ipavich, F. M., *Nature* **318**, 426-429 (1985).
11. Geiss, J., Gloeckler, G., Mall, U., von Steiger, R., Galvin, A. B., and Ogilvie, K. W., *Astron. Astrophys.* **282**, 924-933 (1994).
12. Adams, J. H. Jr. et al., *Astrophys. J. Letters* **375**, L45-L48 (1991).
13. Klecker, B. et al., *Astrophys. J. Letters* **442**, L69-L72 (1995).
14. Cummings, A. C. et al., *Geophys. Res. Letters* **22**, 341-344 (1995).
15. Trattner, K. J., Marsden, R. G., Bothmer, V., Sanderson, T. R., Wenzel, K.-P., Klecker, B., and Hovestadt, D., *Astron. Astrophys.* **316**, 519-527 (1996).
16. Stone, E. C., *Proc. 20th Internat. Cosmic Ray Conf. (Moscow)* **7**, 105-114 (1987).
17. Stone, E. C., Cummings, A. C., Hamilton, D. C., Hill, M. E., and Krimigis, S. M., *Proc. 26th Internat. Cosmic Ray Conf. (Salt Lake City)* **7**, 551-554 (1999).

18. Takashima, T. et al., *Astrophys. J. Letters* **477**, L111-L113 (1997).

19. Reames, D. V., *Astrophys. J.* **518**, 473-479 (1999).

20. Cummings, A. C., Stone, E. C., and Steenberg, C. D., *Proc. 26th Internat. Cosmic Ray Conf. (Salt Lake City)* **7**, 531-534 (1999).

21. Mewaldt, R. A., Selesnick, R. S., Cummings, J. R., Stone, E. C., and von Rosenvinge, T. T., *Astrophys. J. Letters* **466**, L43-L46 (1996).

22. Klecker, B., Oetliker, M., Blake, J. B., Hovestadt, D., Mason, G. M., Mazur, J. E., and McNab, M. C., *Proc. 25th Internat. Cosmic Ray Conf. (Durban)* **2**, 273-276 (1997).

23. Jokipii, J. R., in *Acceleration and Transport of Energetic Particles Observed in the Heliosphere*, AIP Conf. Proc. this volume, New York: AIP Press (2000).

24. Barghouty, A. F., Jokipii, J. R., and Mewaldt, R. A., in *Acceleration and Transport of Energetic Particles Observed in the Heliosphere*, AIP Conf. Proc. this volume, New York: AIP Press (2000).

25. Steenberg, C. D., in *Acceleration and Transport of Energetic Particles Observed in the Heliosphere*, AIP Conf. Proc. this volume, New York: AIP Press (2000).

26. Mewaldt, R. A. et al., *Geophys. Res. Letters* **20**, 2263-2266 (1993).

27. Stone, E. C. et al., *Space Sci. Rev.* **86**, 357-408 (1998).

28. von Rosenvinge, T. T. and Paizis, C., *Proc. 17th Internat. Cosmic Ray Conf. (Paris)* **10**, 69-72 (1981).

29. Teegarden, B. J., McDonald, F. B., and Balasubrahmanyan, V. K., *Acta Physica Hungarica* **29**, Suppl. 1, 345 (1970).

30. Mogro-Campero, A., Schofield, N., and Simpson, J. A., *Proc. 13th Internat. Cosmic Ray Conf. (Denver)* **1**, 140-145 (1973).

31. Jokipii, J. R., in *Physics of the Outer Heliosphere*, S. Grzedzielski and D. E. Page, eds., Oxford: Pergamon Press (1990).

32. Stone, E. C. et al., *Space Sci. Rev.* **86**, 285-356 (1998).

33. Klecker, B. et al., *Space Sci. Rev.* **83**, 259-308 (1998).

34. Hasebe, N. et al., *Geophys. Res. Letters* **21**, 3027-3030 (1994).

35. Mewaldt, R. A., Cummings, J. R., Leske, R. A., Selesnick, R. S., Stone, E. C., and von Rosenvinge, T. T., *Geophys. Res. Letters* **23**, 617-620 (1996).

36. Oetliker, M., Klecker, B., Mason, G. M., McNab, M. C., and Blake, J. B., *Proc. 25th Internat. Cosmic Ray Conf. (Durban)* **2**, 277-280 (1997).

37. Fahr, H. J., Ripken, H.W., and Lay, G., *Astron. Astrophys.* **102**, 359-370 (1981).

38. Geiss, J., Gloeckler, G., and von Steiger, R., *Space Sci. Rev.* **78**, 43-52 (1996).

39. Mewaldt, R. A., *Proc. 26th Internat. Cosmic Ray Conf. (Salt Lake City)* **7**, 547-550 (1999).

40. Leske, R. A., in *Summary-Rapporteur Vol. of the 26th Internat. Cosmic Ray Conf.*, B. Dingus, ed., New York: AIP Press (2000), in press.

41. Christian, E. R. et al., *Proc. 26th Internat. Cosmic Ray Conf. (Salt Lake City)* **7**, 559-560 (1999).

42. Anders, E. and Grevesse, N., *Geochim. Cosmochim. Acta* **53**, 197-214 (1989).

43. Geiss, J., Buehler, F., Cerruti, H., Eberhardt, P., and Filleux, Ch., *Apollo 16 Prelim. Sci. Report, NASA SP-315* **231**, 14-1–14-10 (1972).

44. Podosek, F. A., *Ann. Rev. Astron. Astrophys.* **16**, 293-334 (1978).

45. Connell, J. J. and Simpson, J. A., *Proc. 23rd Internat. Cosmic Ray Conf. (Calgary)* **1**, 559-562 (1993).

46. Lukasiak, A., Ferrando, P., McDonald, F. B., and Webber, W. R., *Astrophys. J.* **426**, 366-372 (1994).

47. Leske, R. A., Mewaldt, R. A., Cummings, A. C., Cummings, J. R., Stone, E. C., and von Rosenvinge, T. T., *Space Sci. Rev.* **78**, 149-154 (1996).

48. Roederer, J. G., *Dynamics of Geomagnetically Trapped Radiation*, New York: Springer (1970).

49. Cummings, J. R., Cummings, A. C., Mewaldt, R. A., Selesnick, R. S., Stone, E. C., and von Rosenvinge, T. T., *Geophys. Res. Letters* **20**, 2003-2006 (1993).

50. Leske, R. A., Cummings, J. R., Mewaldt, R. A., Stone, E. C., and von Rosenvinge, T. T., in *High Energy Solar Physics*, AIP Conf. Proc. 374, R. Ramaty, N. Mandzhavidze, and X.-M. Hua, eds., New York: AIP Press, 86-95 (1996).

51. Leske, R. A., Cummings, J. R., Mewaldt, R. A., Stone, E. C., and von Rosenvinge, T. T., *Astrophys. J. Letters* **452**, L149-L152 (1995).

52. Selesnick, R. S., Mewaldt, R. A., and Cummings, J. R., *Proc. 25th Internat. Cosmic Ray Conf. (Durban)* **2**, 269-272 (1997).

53. Jokipii, J. R., *Astrophys. J. Letters* **466**, L47-L50 (1996).

54. Grigorov, N. L. et al., *Geophys. Res. Letters* **18**, 1959-1962 (1991).

55. Mewaldt, R. A., Selesnick, R. S., and Cummings, J. R., in *Radiation Belts: Models and Standards*, Geophys. Monograph 97, J. F. Lemaire, D. Heynderickx, and D. N. Baker, eds., Washington, D.C.: AGU Press, 35-41 (1996).

56. Blake, J. B. and Friesen, L. M., *Proc. 15th Internat. Cosmic Ray Conf. (Plovdiv)* **2**, 341-346 (1977).

57. Selesnick, R. S., Cummings, A. C., Cummings, J. R., Mewaldt, R. A., Stone, E. C., and von Rosenvinge, T. T., *J. Geophys. Res.* **100**, 9503-9518 (1995).

58. Selesnick, R. S. et al., *Geophys. Res. Letters*, submitted.